Short article

Developmental Cell

# Myocardium and endocardium of the early mammalian heart tube arise from independent multipotent lineages specified at the primitive streak

## Graphical abstract

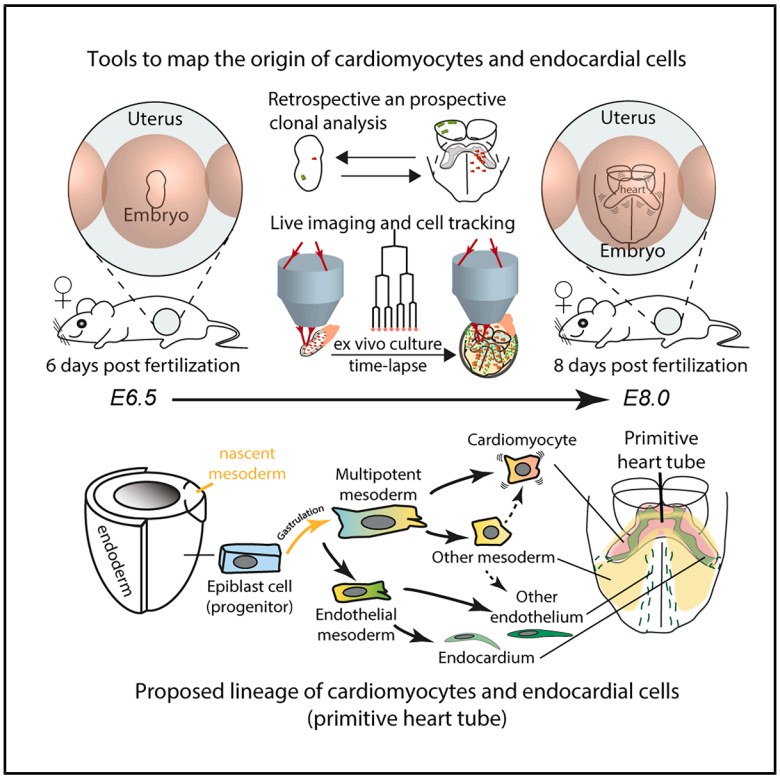


## Highlights

- Multi-approach, unbiased cell lineage analysis is reported in early mouse embryos
- The primitive heart does not assemble from cardiac-specific progenitors
- Endo- and myocardial fates segregate at gastrulation but keep multipotentiality
- Endo- and myocardial precursors gastrulate and migrate together to form the heart

## Authors

Miquel Sendra, Katie McDole, Juan de Dios Hourcade, ..., Philipp J. Keller, Jorge N. Domínguez, Miguel Torres

## Correspondence

miquel.sendra@cnic.es (M.S.), mtorres@cnic.es (M.T.)

## In brief

Sendra et al. use clonal analysis and live imaging in mouse embryos to show that the primitive heart arises from two multipotent mesodermal populations, not a cardiac-specific precursor. Myocardial and endocardial lineages segregate at gastrulation, but keep multipotentiality, challenging the current views on the emergence of early cardiac cell lineages.

Sendra et al., 2025, Developmental Cell *60*, 2434–2444
September 22, 2025 
https://doi.org/10.1016/j.devcel.2025.05.002

CellPress

CellPress
OPEN ACCESS

Developmental Cell

Short article

# Myocardium and endocardium of the early mammalian heart tube arise from independent multipotent lineages specified at the primitive streak

Miquel Sendra,[1,*] Katie McDole,[2] Juan de Dios Hourcade,[1] Susana Temiño,[1,3] Morena Raiola,[1] Léo Guignard,[4] Philipp J. Keller,[5] Jorge N. Domínguez,[3,6] and Miguel Torres[1,3,7,*]

[1]Fundación Centro Nacional de Investigaciones Cardiovasculares Carlos III (CNIC), 28029 Madrid, Spain
[2]MRC Laboratory of Molecular Biology, Cambridge Biomedical Campus, Cambridge CB2 0QH, UK
[3]Centro de Investigación Biomédica en Red de Enfermedades Cardiovasculares (CIBERCV), 28029 Madrid, Spain
[4]CNRS, UTLN, LIS 7020, Turing Centre for Living Systems, Aix Marseille University, Marseille, France
[5]Janelia Research Campus, Howard Hughes Medical Institute, Ashburn, VA 20147, USA
[6]Department of Experimental Biology, Faculty of Health Sciences University of Jaén, Jaén 23071, Spain
[7]Lead contact
*Correspondence: miquel.sendra@cnic.es (M.S.), mtorres@cnic.es (M.T.)
https://doi.org/10.1016/j.devcel.2025.05.002

## SUMMARY

The formation of the primitive heart tube from cardiomyocytes and endocardial cells is a key event in mammalian development. Previous studies suggested that cardiomyocytes and endocardial cells segregate from a shared cardiac progenitor around the onset of gastrulation, yet their lineage relationship with other mesodermal tissues remains unclear. Using retrospective and prospective clonal analyses in mouse embryos, we traced cardiomyocyte and endocardial progenitors from the primitive streak to the heart tube. Our results identify two independent mesodermal populations specified around gastrulation onset. While each of these populations is unipotent in producing cardiomyocytes or endocardium, they retain multipotency and contribute to different subsets of non-cardiac mesoderm. Nonetheless, live imaging identifies simultaneous ingression and intermingling of these two mesodermal lineages in the primitive streak, showing their coordinated specification and migration. The proposed model for cardiac progenitor specification will help understanding the origins of congenital heart diseases and designing tissue engineering strategies.

## INTRODUCTION

The primitive heart tube is the first functional organ in the mammalian embryo. This rudimentary heart assembles and starts pumping nutrients shortly after gastrulation. It contains two cell types: cardiomyocytes (CMs), which form the muscular wall, and endocardial cells (ECrs), which are specialized endothelial cells lining the cardiac lumen.[1] ECrs form a continuum with the embryonic vasculature, are involved in forming trabeculae,[2] contribute to the formation of cardiac valves and septa[3] and differ from other endothelial cells in gene expression profile.[4,5] CM and ECr precursors are located at embryonic day (E) 7.75 within the anterior splanchnic mesoderm, forming a horseshoe-shaped structure known as the cardiac crescent, from which the primitive heart tube develops.[1]

Finding when and where cell fates are specified is crucial to understanding how the primitive heart forms with the correct number and arrangement of CMs and ECrs. In developmental biology, cells are considered ''specified'' when they consistently produce a particular type. Clonal analysis addresses the specification status of targeted cells[6]: by labeling single cells at different developmental stages and examining their progeny, the timing of cell lineage specification and the presence of precursors with diverse potentialities can be characterized. For instance, identification of progenitors that give rise to both CMs and ECrs indicates lack of specification to either fate at the time of labeling, but it could reveal specified bipotential cardiac precursors, if such contribution was systematically found at a given stage. Prospective clonal analysis involves labeling cells at known developmental stages and locations to track the contribution of their progeny. In contrast, retrospective clonal analysis uses genetic labeling *in utero* and examines only the final contribution of the progeny.

Clonal analysis experiments in zebrafish, chicken, and mouse models have traced the location of heart progenitors and pointed to an early specification of CMs and ECrs, occurring around the onset of gastrulation. In chicken embryos, the rostral half of the primitive streak contains both cardiac progenitors, which are already specified to form either CM or ECr progenies.[7,8] Retrospective clonal analysis in mouse embryos also suggests an early specification. Genetically labeled *Mesp1*-expressing cells around the onset of gastrulation (~E6.5) give rise to cell clusters in the left ventricle—a heart chamber derived from the primitive heart tube—containing either only CMs or ECrs, indicating early

 

specification of progenitors.[9,10] However, up to a quarter of *Mesp1*-expressing clones labeled at ~E7.25 gave rise to mixed progenies in the right ventricle, indicating that later progenitors can give rise to both CMs and ECrs.[9,10] Together, this suggests that the CM and ECr lineages segregate early during gastrulation in the primitive streak, but some progenitors that differentiate later retain the capacity to contribute to both lineages. These studies, however, did not investigate whether early progenitors also contributed to cells outside the heart. Therefore, the lineage decisions tree remains unclear, and it is not known whether progenitors are exclusively cardiac or also give rise to mesodermal lineages outside of the heart.

In this context, the lineage relationship between CMs, ECrs, and other mesodermal lineages is controversial. Genetic lineage tracing of cells expressing mesodermal transcription factors and *in vitro* studies on stem cell differentiation support the idea that CMs and ECrs arise from a cardiac-specific common progenitor.[11–16] In contrast, zebrafish mid-blastula clones containing both CMs and ECrs also give rise to blood vessels and blood cells,[17] and endocardium is contributed by vascular endothelial progenitors in avian embryos,[18] suggesting that a cardiac-exclusive progenitor rarely exists. An alternative lineage tree proposes that ECrs derive from hematopoietic/vascular progenitors and then migrate to populate the developing heart tube in zebrafish embryos.[19,20]

To understand how CMs, endothelial cells, and other mesodermal lineages are related, we used three unbiased clonal analysis methods in mouse embryos, none of which relied on lineage-specific Cre drivers: (1) retrospective clonal analysis using *RNApol2*-driven (ubiquitous) expression of *CreERT2*, combined with low doses of 4-OH tamoxifen to achieve sparse recombination of floxed *tdTomato* and e*GFP* reporters. (2) Prospective clonal analysis using TAT-Cre microinjection to recombine these same reporters in single cells. (3) Live imaging of mouse embryos developing from pre-streak (E6.5) to primitive heart tube formation (E8.0) for complete spatiotemporal reconstruction of CM and ECr lineages. Our findings confirm a predominant event of CMs versus ECrs lineage specification around the onset of gastrulation, with few progenitors at later stages retaining the ability to generate both cell types of the primitive heart tube. Moreover, we found no evidence supporting the existence of a cardiac-exclusive progenitor pool at any stage. Instead, our data suggest that CMs and ECrs originate independently from cell populations specified in the late epiblast/early mesoderm that retain ability to multifurcate into distinct non-cardiac lineages. Our observations challenge the view of cardiac-specific progenitors as the main source of the myocardium and endocardium for the primitive heart tube.

## RESULTS

### Unbiased labeling of mouse embryonic progenitors reveals lineage restriction in the primitive heart tube

We conducted a random, lineage-unrestricted clonal analysis using a tamoxifen-inducible ubiquitous driver—*RNApol2:CreERT2*—and a two-reporter strategy[21–25] (STAR Methods). We adjusted the tamoxifen dose to target single cells during the ~E6.25 to E6.75 period and analyzed the contribution of their progenies in whole embryos at E8.0–E8.25 (Figures 1A and 1B). From 737 embryos generated, we focused on 44 showing fluorescence in the cardiac region containing a total of 46 labeled cell clusters. According to the two-reporter strategy statistics, 94.5% of monocolor cell clusters were expected to be derived from single cells (Figures S1A–S1C; STAR Methods). We analyzed the contribution of each cluster to different embryonic compartments by immunostaining for sarcomeric myosin heavy chain (MF20) and ERG (ETS-related gene)[26] followed by confocal imaging to identify CMs and endothelial cells (Figure 1C).

To investigate the timing of CM and ECr specification, we estimated the embryonic stage at which recombination occurred. The induction time of each clone was estimated by calculating the time required to generate its number of cells according to the reported average cell division rate during the embryonic stages E6.5–E8.5[27,28] and subtracting this time from the actual stage at dissection (Figures S1D and S1E; STAR Methods). Our estimation aligned with the reported pharmacodynamics of 4-OH tamoxifen in mouse blood, which peaks around 12 h after injection (Figure S1F). In addition, the scoring of bilateral clones, which only result from progenies labeled before mesoderm ingression,[29] identified the timing of primitive streak ingression for cardiac progenitors around E6.75 and confirmed the validity of the staging approach (Figures S1G–S1I). The chronological ordering of clones revealed that inductions resulting in progenitors that produced both CMs and ECrs occurred at early induction times and disappear rapidly between E6.75 and E7.0 (Figure 1D). In most cases, the clones containing both CMs and ECrs also contributed to other mesoderm regions outside the primitive heart tube (18 out of 20; Figures 1F, 1G, and S1J). These results question the idea of an exclusive cardiac bipotential progenitor and suggest cardiac precursors are multipotent. Furthermore, the fact that a substantial fraction of clones induced before E6.75 (9/24) do not show common contribution to CMs and ECrs (Figures 1D and S1J) discards the idea of a transient bipotential precursor as a necessary route for the specification of these two heart lineages. These results thus suggest that most mesodermal progenitors get specified to exclusively contribute either CMs or ECrs during a short time period around their recruitment to the primitive streak; however, despite this restriction, they remain able to generate non-cardiac mesodermal tissues.

### TAT-Cre microinjection reveals a higher multi-lineage potential in the epiblast compared with the nascent mesoderm

Next, we performed prospective clonal analysis by TAT-Cre microinjection,[30] which allowed us to recombine single cells at custom stages and embryonic locations, and cultured the embryos to analyze the resulting clones in the heart (Figures 2A, 2B, and 2E). We obtained clones contributing to both CMs and endocardium at high frequency (5/7) when injecting pre-streak embryos and at lower frequency (1/7) when injecting early- and middle-streak embryos, whereas later injections always labeled separate lineages (Figures 2C, 2E, and S2A). These results suggest that the endocardial and CM lineages are already independent at the time of their ingression in the primitive streak (~mid-streak). In addition, injections in proximal or distal regions of the primitive streak did not result in

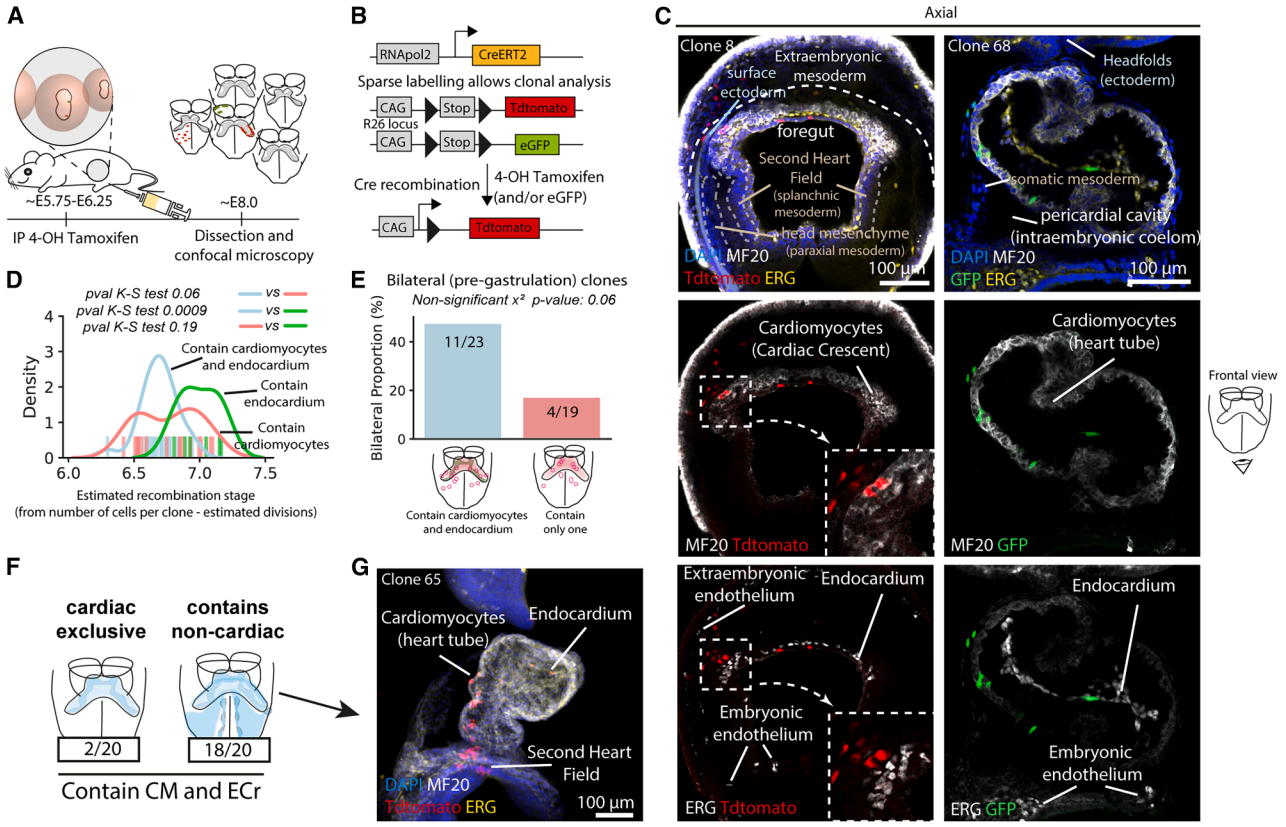


**Figure 1. Retrospective clonal analysis reveals independent specification of endothelial and CM lineages in the heart**

(A) Clonal analysis strategy.

(B) CreERT2 expression from the ubiquitous *RERT* allele[25] and dual *Rosa26* reporter alleles (tdtTomato and GFP) track Cre activity.

(C) Whole-mount confocal images showing clonal contributions to mesodermal locations, with MF20 and ERG staining distinguishing CMs and endothelial cells (endocardial cells [ECr]).

(D) Kernel density estimation (KDE) plot of recombination stage for 46 clones ($n$ = 44 embryos, Kolmogorov-Smirnov test).

(E) Proportion of bilateral (pre-gastrulation) clones contributing to CM + ECr or CM/ECr separately (chi-squared test, n.s.).

(F) Number of clones containing CM + ECr alone versus CM + ECr + other mesoderm.

(G) Example of a tamoxifen-induced clone with CM, ECr, and other mesoderm at E8.5.

Source data: Data S1.

differences in contributions to mixed CM + ECr progenies, which suggests a similar likelihood of finding multipotent or specified progenitors in either region (Figures 2D and S2B). Clones that showed mixed progenies also contained cells outside of the primitive heart tube, which is consistent with the low frequency of CM + ECr-exclusive clones in the retrospective analysis. Together, the retrospective and prospective clonal analyses suggest that CMs and ECrs are specified by independent mechanisms rather than via a cardiac-specific progenitor.

## Spatiotemporal mapping and lineage reconstruction of CM and endocardium progenitors

To better understand the emergence of the CM and endocardial lineages, we used live imaging to track cardiac progenitors from ~E6.5 to their differentiation in the cardiac crescent at ~E8.0. Adapting our previous protocol,[31,32] we conducted time-lapse 3D imaging using two-photon microscopy and random cell lineage tracing using *RNApol2:CreERT2* inducer and the *tdTomato*$^{flox/flox}$ and *mTmG* reporter alleles[23,25,33] (Figures S3A and S3B). Additionally, we used a *CBF1-Venus* allele to identify endothelial cells at later time points[34] (Figure S3C). First, based on tissue morphology, we identified the cardiac crescent region at the final time points of the videos. Second, we distinguished CMs as rounded cells forming a chamber and ECrs as Venus-positive elongated cells within the chamber lumen (Figure S3D). Finally, we manually tracked back CMs and ECr lineages to the beginning of the videos using the MaMut ImageJ plugin.[35] We applied this strategy to analyze four embryos using the Tomato reporter for lineage tracing in a two-photon microscope (MS1-MS4). In addition, we analyzed two *H2B:miRFP703* embryos (KM1 and KM2) with ubiquitous nuclear fluorescence in a light-sheet microscope[29,36] using the nuclear detection for cell lineage tracing (Videos S1, S2, S3, S4, S5, S6, and S7).

By detecting cell divisions during tracking, we reconstructed the lineages of 55 individual progenitors in the nascent mesoderm surrounding the primitive streak or in the epiblast (Figures 3 and S4). After excluding lost tracks, these progenitors were linked to 388 descendant cells at the end of the time-lapse sequences (Figures 3B and S4B). Among the progenies studied, we found

CellPress
OPEN ACCESS

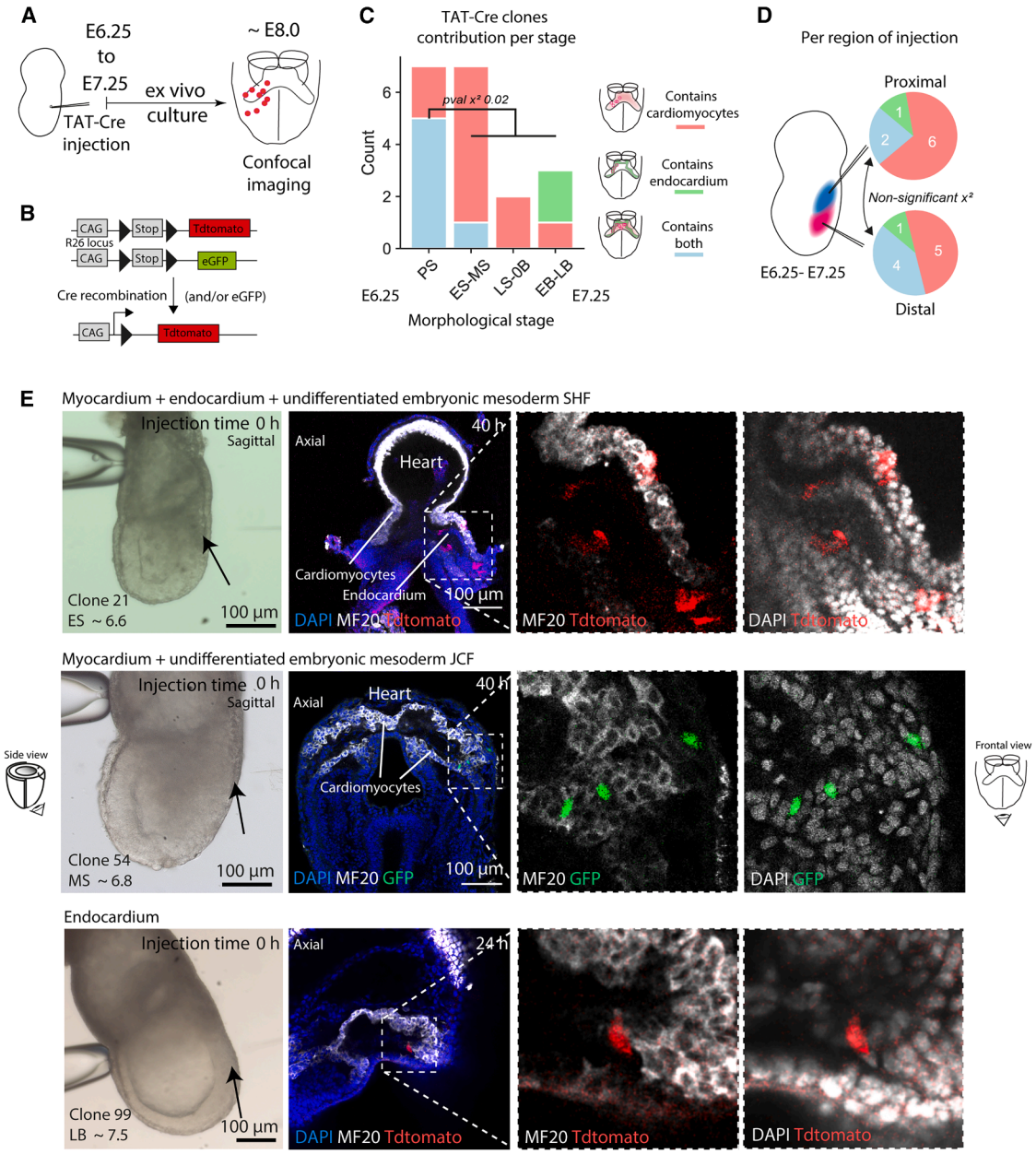


**Figure 2. TAT-Cre microinjection for prospective clonal analysis of primitive heart tube progenitors**

(A) Experimental setup for TAT-Cre-induced clonal analysis.

(B) Recombination strategy using floxed reporters.

(C) Distribution of clones contributing to CM + ECr or CM/ECr separately across developmental stages. A chi-squared test showed significant differences in CM + ECr clone numbers between pre-streak and later embryos.

(D) Clone distribution by proximal vs. distal injection sites. A chi-squared test found no significant difference in CM + ECr clone proportions.

(E) Examples of TAT-Cre-induced clones. Top: a progenitor contributing to CMs, endocardium, and undifferentiated mesoderm. Middle: zoom-ins of recombined cells inside and outside the primitive heart tube (MF20 staining). Bottom: a clone giving rise to endocardium.

Source data: Data S1.

only three progenitors yielding both CMs and ECrs. In total, we identified 23 CM, 21 endothelial, and three mixed CM + ECr progenitors. In 2 of the 3 cases of bi-potentiality, the fates segregated at the last division before becoming mesenchymal at the primitive streak (Figure S4B), and a third one did so one division later (Figure 3B). In line with the clonal analyses, live cell tracking shows that the CM and endocardial lineages are largely segregated at the beginning of the time-lapse study.

In addition, the live imaging data provided spatiotemporal information of CM and endocardial progenitors. We then used this information to map the positions of the progenitors at their exit from the primitive streak in the nascent mesoderm. This

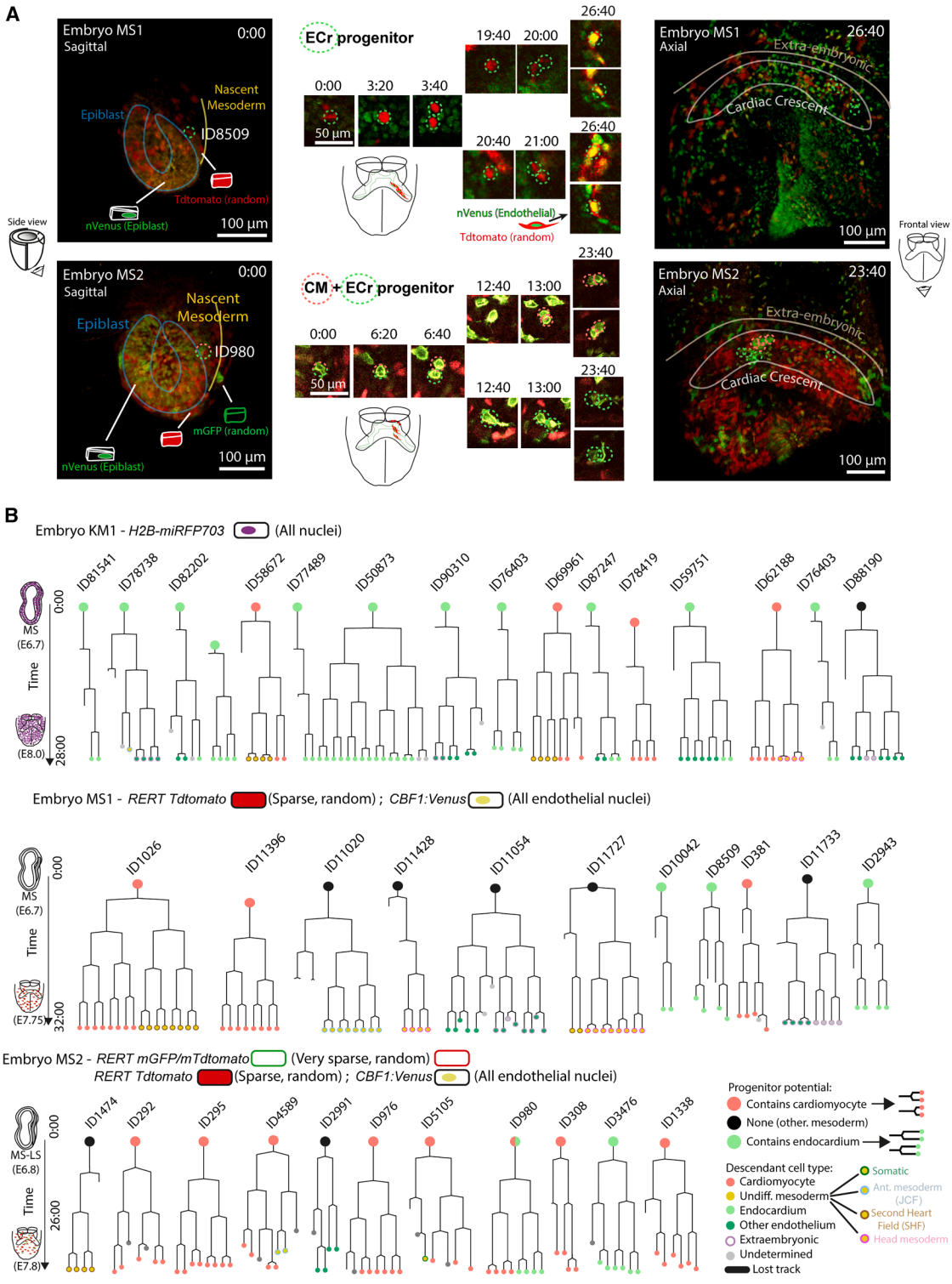


**Figure 3. Two-photon time-lapse microscopy for cardiac progenitor tracking and lineage reconstruction**

(A) Example of two tracked cells. Initial and final time points are shown as maximal intensity projections. Optical planes display individual cells and their progeny after division. Timestamps indicate h:min.

(B) Reconstructed lineage trees from the earliest progenitor to cell descendants. Endpoint cell fates are shown as colored circles; progeny cell types as smaller colored circles. Each branch bifurcation represents a cell division event ($n$ = 41 and 286 cells at initial and final time points, respectively, from 3 embryos).

study revealed no spatial segregation between precursors destined to either fate (Figure S3E). Despite being already segregated, CM and ECr progenitors thus arise simultaneously from the same primitive streak region, which suggests that they are exposed to equivalent signaling environments at this point. This observation reinforces the idea of the early specification of single precursors toward lineages that generate either ECrs or CMs but not both, despite sharing the same environment.

## Lineage relationships of CMs and ECrs with other mesodermal tissues

The three clonal analysis techniques provided insights into the timing and location of the cell progenitors able to produce CMs and ECrs; however, we also found that the contributions of these lineages were not cardiac-specific. Here, we studied the lineage relationships between the cardiac cells and other mesodermal tissues. To address this, we integrated data from all three methods, encompassing 103 clones containing either CMs, ECrs, or both. We ordered these clones by their estimated birth date, determined by either the estimated recombination timing or the start of live imaging cell tracking (Figures 4A and S5; STAR Methods). Our clone collection contributes in total 1,072 CMs and 613 ECrs in the E8 heart tube. A primitive heart tube at this stage typically contains 690 CMs and 180 ECrs on average (Figure S6A). Therefore, our sample includes 1.5 times and 3 times the average numbers of CMs and ECrs found in an embryo, respectively, ensuring comprehensive coverage of progenitors, including rare populations. Between the middle-streak stage (MS, E6.75) and primitive heart tube formation, CMs and ECrs progenitors undergo an average of four divisions in the time-lapse analyses (Figure S6B). This indicates that the total progenitor pool is composed of at least 170 CM and 45 ECr specified progenitors at the MS stage. Given that some progeny of these specified progenitors contributes to tissues outside the primitive heart tube, the required number at MS for primitive heart formation may be higher. As expected, bilateral (pre-mesoderm ingression) clones were found to contain larger cell numbers (Figure S6C). Additionally, we calculated the probability that CM-only or ECr-only clones appear by chance rather than through specification. The likelihood of clones contributing exclusively to CM or ECr by chance averaged 3% for CM and less than 1% for ECr, and 91% of clones had a probability of less than 0.05 of having only CM or ECr purely by chance, indicating that the majority of these clones represent specified progenitors (Figure S6D).

To quantify lineage relationships, we then calculated the Jaccard similarity score between CM, ECr, and each of the non-cardiac cell types scored (Figure 4B). This analysis revealed a weak lineage relationship between CMs and ECrs. Instead, CMs shared a closer lineage relationship with undifferentiated mesoderm, while ECrs were related to other embryonic endothelial cells (Figures 4B and S5). Next, we analyzed the extra-cardiac contributions of clones classified by their contributions to CM and/or ECr. Most of the clones that contained both CM and ECr also contributed to other mesodermal tissues outside the heart (87%, 28/32 clones), with a minority of clones exclusively containing CM and ECr (Figures 4C and S5), which agrees with the early origin and multipotentiality of this set of clones. Clones contributing to CM but not ECrs were more restricted, yet 63% (31/49) of them still showed contribution to extra-cardiac mesoderm. In contrast, only 23% (5/22) of clones contributing to ECr but not CM also contributed to extra-cardiac mesoderm. In this case, all 5 clones containing extra-cardiac mesoderm contained non-cardiac endothelium, and three of them exclusively contained non-cardiac endothelium. Taking this into account, 91% of the clones containing ECr but not CM were restricted to the endothelial lineage. These results indicate a different set of lineage relationships for primary endocardium versus myocardium, with ECr precursors much more restricted to an endothelial fate than CM precursors.

Next, we examined the subtypes of undifferentiated mesoderm associated to clones contributing to CM, ECr, or both (Figures 4D and S5). We found that in both CM + ECr and CM clones, the contribution to non-cardiac mesoderm was similar and widespread, with higher contributions to the juxta-cardiac field (JCF) and second heart field (SHF), followed by somatic mesoderm, head mesoderm, and paraxial mesoderm. Given that at the final stages analyzed the contribution of the juxta-cardiac field to the myocardium has already taken place,[37,38] these results show that a majority of clones (73%; 40/55) are not restricted to a cardiac fate (SHF; Figure S5). In fact, the distribution of the contributions seems to relate to the physical proximity of the different regions, rather than to their identity. The low number of ECr clones that also show other mesoderm (2) precludes any statistical conclusion about their contribution (Figure 4E). In addition, ECr showed a greater spatial extension than CM in CM + ECr clones (Figures S6E–S6G). These results support the idea of the specification of CM and ECr from a multipotent mesodermal precursor and not from a cardiac progenitor.

We next analyzed the timing of the segregation of the CM and ECr lineages considering the whole clone collection. Before the cardiac precursors start gastrulation (E6.75), we observed 53% (23/43) of clones contributing to both CMs and ECrs. This proportion reduced to 22% (7/32) during the period of cardiac precursor gastrulation (E6.75–E7.0) and dropped to 4% (1/28) after E7.0. Regarding the timing of segregation of the CMs and ECr lineages from other mesoderm, 70% of the clones induced before E6.75 and containing CM or ECr, but not both, contributed to non-cardiac, non-endothelial tissues (14/20; Figure S5). Between E6.75 and E7.0 this proportion reduced to 52% (14/25), whereas within those induced beyond E7.0 it dropped to 14% (4/27; Figure S5). Temporal mapping of the earliest CM- or ECr-exclusive precursors revealed no staging differences, suggesting simultaneous restriction of the cardiac-specific fate (Figure 4F). These findings suggest that CMs and ECrs are specified independently in the primitive streak, rather than originating from a common cardiac-specific progenitor. Despite contributing to only one of the primitive cardiac fates, these two diverting lineages retain the ability to contribute to other mesodermal fates of the early mouse embryo.

In conclusion, our data show that mesodermal progenitors rapidly specify during gastrulation into multipotent lineages that independently give rise to CMs and ECrs, which are later co-recruited to differentiate in the cardiac crescent and form the primitive heart tube (Figure 4G).

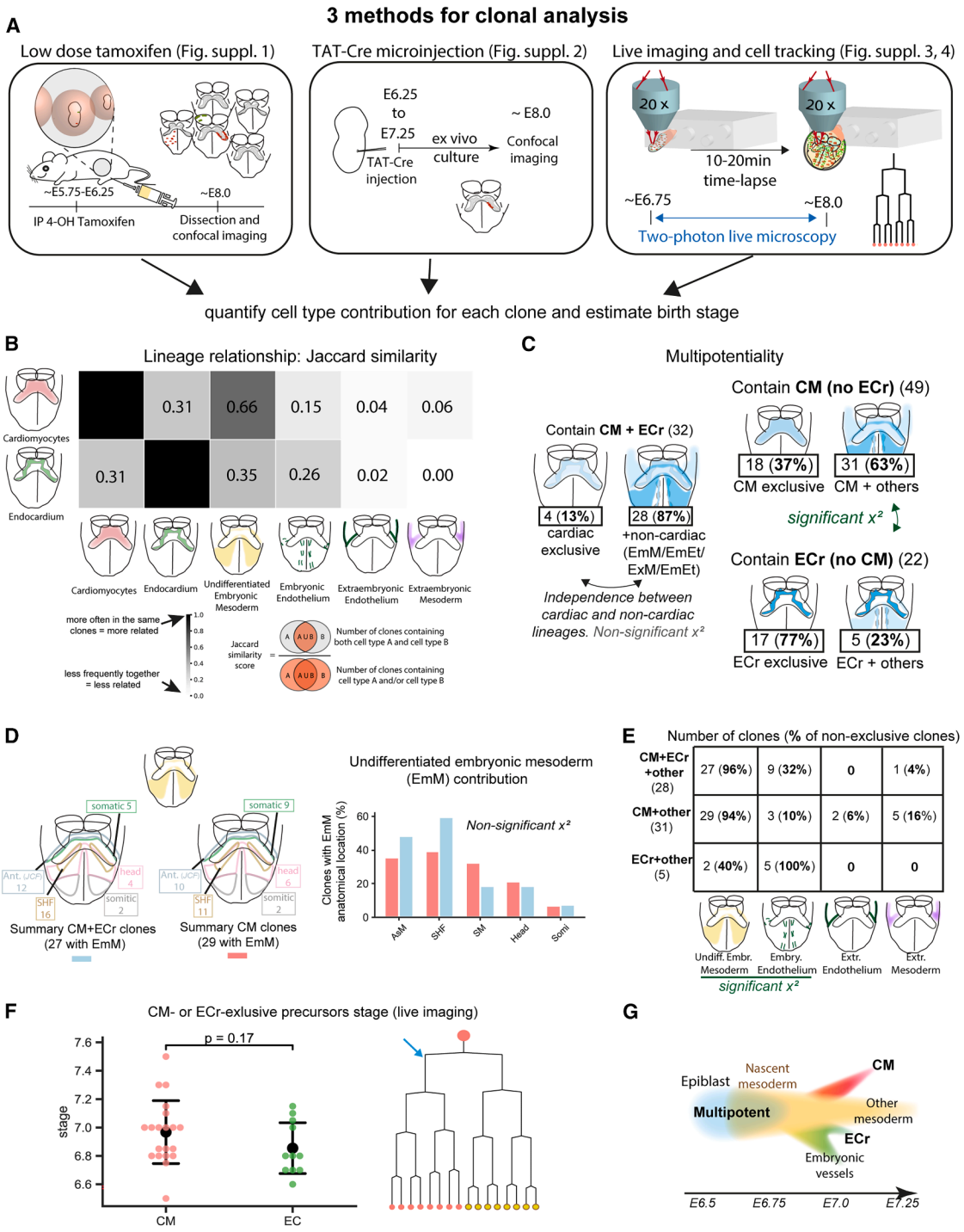


**Figure 4. Clonal analysis reveals lineage relationships between CMs, ECrs, and other mesodermal tissues**

(A) Schematics of three clonal analysis methods.

(B) Heatmap of Jaccard similarity scores between CM, ECr, and other cell types ($n$ = 103 clones).

(C) Degree of cell type exclusivity in CM vs. ECr clones.

(D) Contribution of CM + ECr and CM clones to undifferentiated embryonic mesoderm regions (chi-squared test for independence).

(E) Non-cardiac composition of CM + ECr, CM, and ECr clones.

(F) Temporal mapping of the earliest CM- or ECr-exclusive precursors ($n$ = 21 CM and 11 ECr clones, 6 embryos).

(G) Proposed lineage decision tree showing multipotent mesodermal progenitors as the origin of the primitive heart tube.

Source data: Data S1.

## DISCUSSION

Using clonal analysis and live imaging to track single-cell progenies, we found that the primitive heart tube derives from pluripotent progenitors in the epiblast that get specified to either contribute to CMs or ECrs in the nascent mesoderm. Upon their recruitment to the primitive streak, they become restricted from contributing to both ECrs and CMs and are able to contribute to only one of these lineages. Paradoxically, while they show this early restriction, they independently keep the ability to contribute to non-cardiac fates. These observations challenge the idea of a bipotential cardiac-exclusive progenitor population as the origin of CMs and ECrs. Our results do not exclude the possibility that during a narrow time window, some cardiac-exclusive bipotent progenitors exist, but the low frequency of cardiac-exclusive progenitors (13% of CM + ECr clones and 4% of all clones) argues against this source as a significant pathway for the generation of primitive cardiac lineages. Our results instead suggest a rapid transition from pluripotency to multipotency in the primitive streak with segregation of at least two lineages, one retaining the ability to generate CMs but not ECrs and another one retaining the ability to generate ECrs but not CMs. While both remain multipotent, that of ECrs becomes much more restricted to the endothelial fate, while that of CMs retains good ability to contribute to multiple mesodermal fates. A second rapid transition from multipotency to unipotency occurs during primitive heart formation. The fact that the ECr fate is highly related to other endothelial fates suggests a strong bias of the mesodermal lineage contributing to ECr to also contribute to different endothelia. An interesting possibility is that endocardial progenitors may first acquire a broader endothelial identity and then acquire the endocardial fate upon reaching the cardiac primordium. Single-cell RNA sequencing has identified *Notch1* as a potential early marker of endothelial *Mesp1*+ progenitors at E7.25, with *Erg* emerging during its establishment.[39] Immunostaining for activated Notch1 (N1ICD) and ERG shows their presence in both extraembryonic regions and anterior mesoderm as early as E7.25 for ERG, with N1ICD appearing later, aligning with the position of tracked endocardial progenitors and *CBF1:Venus* transgene expression (Figure S7). However, specific endocardial markers, such as *Nfatc1*, emerge later, around E7.75–E8.0.[5] This temporal progression suggests an initial pan-endothelial state for endocardial progenitors, which is further refined upon integration into the cardiac crescent and heart tube.

Myocardial clones are strongly associated with contributions to all mesodermal types surrounding the cardiac crescent and predominantly, to JCF and SHF. These observations could be interpreted as resulting from the dispersion of multipotent mesodermal precursors that then diversify according to the environment that they find at destination. The higher coincidence of common contributions to myocardium, SHF and JCF supports this idea, as these regions are anatomically contiguous. In fact, 73% of myocardial clones contribute to non-myocardial fated regions, which agrees with this interpretation. Interestingly, although there are few clones that contribute to extraembryonic mesoderm, these are mostly associated with CM-contributing clones, which might be related to the shared transcriptional profiles of extraembryonic lineages and those CMs that differentiate from the juxta-cardiac field.[37,38]

Therefore, while early mechanisms bias progenitors toward CM or endocardial fates, differentiation cues in the cardiogenic region (anterior part of the embryo) may dictate their terminal recruitment.[40] Rather than a series of binary hierarchical fate decisions involving a cardiac-specific progenitor as an intermediate state, we then propose that the primitive heart tube precursors are specified from independent multipotent mesodermal lineages. Nonetheless, this segregation scheme between the CM and endocardial lineage shows some leakiness, as reported by rare CM + ECr progenitors in the post-streak mesoderm. In the second heart field, in contrast, progenitors remain multipotent for longer periods, contributing blood and lymphatic endothelial cells, CMs, and smooth muscle cells.[21,41–44] This distinction highlights potential differences in lineage specification dynamics between first and second heart field progenitors, as suggested by studies on later-stage *Mesp1*-expressing progenitors.[9,10]

Fate mapping studies show that progenitors of different organs reside in different regions of the epiblast.[45] Different regions of the primitive streak are exposed to gradients of Wnt, BMP, FGF, and Nodal signaling, which influence cell fate decisions during gastrulation. Under this model, spatial and/or temporal segregation of CM and endocardium progenitors in the primitive streak would be expected to allow their independent specification. However, through live imaging, we tracked CM and endothelial cell precursors back to their initial positions in the nascent mesoderm, revealing no spatial or temporal segregation. This suggests that these progenitors arise from intermingled positions in the primitive streak, ruling out differential exposure to morphogens in the primitive streak as a likely mechanism for their specification.[46,47] One possibility is that local cell interactions or stochastic mechanisms pattern the emergence of the endothelial lineage in the epiblast or primitive streak. However, we cannot exclude regional specification in the epiblast followed by subsequent co-recruitment to the same region of the primitive streak.

Our study reports a scheme for understanding the segregation of mesoderm lineages and their coordination for the formation of the heart, the first functional organ in the mammalian embryo.

### Limitations of the study

While our findings support the early segregation of CM and endocardial lineages, certain limitations remain. We have analyzed the results at stages in which full differentiation of the lineages has not yet taken place, and therefore, we may be underestimating the commitment of some clones. For example, in the case of endothelial clones, we cannot discard that accompanying mesodermal cells might be angioblasts fated to the endothelial lineage. Additionally, technical constraints in lineage tracing and live imaging may have influenced clone recovery, limiting the capture of rare progenitor states and introducing potential biases. Future studies with higher temporal resolution and integrated genetic or multiomic approaches will be essential to position these lineage relationships within the broader mesodermal specification framework and extend insights to later progenitor pools, such as the second heart field.

## RESOURCE AVAILABILITY

### Lead contact

Requests for further information and resources should be directed to and will be fulfilled by the lead contact, Miguel Torres (mtorres@cnic.es).

### Materials availability

This study did not generate new unique reagents.

### Data and code availability

- Raw data have been deposited and are publicly available at Zenodo: https://doi.org/10.5281/zenodo.14922060 as of the date of publication.
- All original code used for analysis and figure generation has been deposited and is publicly available at GitHub: https://github.com/MiquelSendra/CardiacLineage (Zenodo: https://doi.org/10.5281/zenodo.15150056).
- Any additional information required to reanalyze the data reported in this paper is available from the corresponding authors contact upon request.

## ACKNOWLEDGMENTS

We thank members of the Torres group for inspiring discussions and advice. We thank members of the Microscopy and Dynamic Imaging, Transgenesis, and Animal Facility CNIC units for excellent support. We thank "La Caixa" Foundation (ID 100010434) for the fellowship that supported M.S. stipend (LCF/BQ/DE18/11670014). We also thank the Company of Biologists for the traveling fellowship that made possible M.S. stay at Janelia Research Institute with K.M., L.G., and P.J.K. (DEVTF181145). This work was funded by grants PGC2018-096486-B-I00 and PID2022-140058NB-C31 from the Agencia Estatal de Investigación to M.T.; European Commission H2020 Program grant SC1-BHC-07-2019. Ref. 874764 "REANIMA" to M.T., Comunidad de Madrid grant P2022/BMD-7245 CARDIOBOOST-CM to M.T. The CNIC Unit of Microscopy and Dynamic Imaging is supported by FEDER "Una manera de hacer Europa" (ReDIB ICTS infrastructure TRIMA@CNIC, MCIN). The CNIC is supported by the Ministerio de Ciencia e Innovación and the Pro CNIC Foundation and is a Severo Ochoa Center of Excellence (Grant number CEX2020-001041-S, funded by MICIU/AEI 10.13039/501100011033).

## AUTHOR CONTRIBUTIONS

Conceptualization, M.S. and M.T.; methodology, M.S., J.N.D., J.d.D.H., and S. T.; software, M.S., L.G., and M.R.; validation, M.S. and J.N.D.; formal analysis, M.S. and J.N.D.; investigation, M.S. and J.N.D.; data curation, M.S. and J.N. D.; writing – original draft, M.S.; writing – review & editing, M.S. and M.T.; supervision, M.T.; project administration, M.T.; and funding acquisition, M.T.

## DECLARATION OF INTERESTS

The authors declare no competing interests.

## STAR★METHODS

Detailed methods are provided in the online version of this paper and include the following:

- KEY RESOURCES TABLE
- EXPERIMENTAL MODEL AND STUDY PARTICIPANT DETAILS
- METHOD DETAILS
  - Embryo retrieval
  - Whole mount embryo immunostaining
  - Confocal microscopy of fixed embryos
  - Retrospective clonal analysis
  - Tamoxifen preparation
  - TAT–Cre prospective clonal analysis
  - Embryo culture and live imaging of gastrulating mouse embryos
- QUANTIFICATION AND STATISTICAL ANALYSIS
  - Cluster cell counting
  - Clonal probability
  - Cell tracking and lineage reconstruction from live imaging data
  - Probability calculation for clone specification

## SUPPLEMENTAL INFORMATION

Supplemental information can be found online at https://doi.org/10.1016/j.devcel.2025.05.002.

Received: July 11, 2024
Revised: February 8, 2025
Accepted: May 6, 2025
Published: May 27, 2025

## REFERENCES

1. Kaufman, M.H., and Navaratnam, V. (1981). Early differentiation of the heart in mouse embryos. J. Anat. *133*, 235–246.
2. Stainier, D.Y.R., Weinstein, B.M., Detrich, H.W., Zon, L.I., and Fishman, M. C. (1995). Cloche, an Early Acting Zebrafish Gene, Is Required By Both the Endothelial and Hematopoietic Lineages. Development *121*, 3141–3150. https://doi.org/10.1242/dev.121.10.3141.
3. Nakajima, Y., Mironov, V., Yamagishi, T., Nakamura, H., and Markwald, R. R. (1997). Expression of smooth muscle alpha-actin in mesenchymal cells during formation of avian endocardial cushion tissue: A role for transforming growth factor β3. Dev. Dyn. *209*, 296–309. https://doi.org/10.1002/(SICI)1097-0177(199707)209:3<296::AID-AJA5>3.0.CO;2-D.
4. Drake, C.J., and Fleming, P.A. (2000). Vasculogenesis in the day 6.5 to 9.5 mouse embryo. Blood *95*, 1671–1679. https://doi.org/10.1182/blood.v95.5.1671.005k39_1671_1679.
5. De La Pompa, J.L., Timmerman, L.A., Takimoto, H., Yoshida, H., Elia, A.J., Samper, E., Potter, J., Wakeham, A., Marengere, L., Langille, B.L., et al. (1998). Role of the NF-ATc transcription factor in morphogenesis of cardiac valves and septum. Nature *392*, 182–186. https://doi.org/10.1038/32419.
6. Conklin, E.G. (1905). Mosaic development in ascidian eggs. J. Exp. Zool. *2*, 145–223. https://doi.org/10.1002/jez.1400020202.
7. Wei, Y., and Mikawa, T. (2000). Fate diversity of primitive streak cells during heart field formation in ovo. Dev. Dyn. *219*, 505–513. https://doi.org/10.1002/1097-0177(2000)9999:9999<::AID-DVDY1076>3.0.CO;2-6.
8. Cohen-Gould, L., and Mikawa, T. (1996). The fate diversity of mesodermal cells within the heart field during chicken early embryogenesis. Dev. Biol. *177*, 265–273. https://doi.org/10.1006/dbio.1996.0161.
9. Lescroart, F., Chabab, S., Lin, X., Rulands, S., Paulissen, C., Rodolosse, A., Auer, H., Achouri, Y., Dubois, C., Bondue, A., et al. (2014). Early lineage restriction in temporally distinct populations of Mesp1 progenitors during mammalian heart development. Nat. Cell Biol. *16*, 829–840. https://doi.org/10.1038/ncb3024.
10. Devine, W.P., Wythe, J.D., George, M., Koshiba-Takeuchi, K., and Bruneau, B.G. (2014). Early patterning and specification of cardiac progenitors in gastrulating mesoderm. eLife *3*, e03848. https://doi.org/10.7554/eLife.03848.
11. Kouskoff, V., Lacaud, G., Schwantz, S., Fehling, H.J., and Keller, G. (2005). Sequential development of hematopoietic and cardiac mesoderm during embryonic stem cell differentiation. Proc. Natl. Acad. Sci. USA *102*, 13170–13175. https://doi.org/10.1073/pnas.0501672102.
12. Chan, S.S.K., Shi, X., Toyama, A., Arpke, R.W., Dandapat, A., Iacovino, M., Kang, J., Le, G., Hagen, H.R., Garry, D.J., et al. (2013). Mesp1 patterns mesoderm into cardiac, hematopoietic, or skeletal myogenic progenitors in a context-dependent manner. Cell Stem Cell *12*, 587–601. https://doi.org/10.1016/j.stem.2013.03.004.
13. Kattman, S.J., Huber, T.L., and Keller, G.M.M. (2006). Multipotent Flk-1+ Cardiovascular Progenitor Cells Give Rise to the Cardiomyocyte,

Endothelial, and Vascular Smooth Muscle Lineages. Dev. Cell *11*, 723–732. https://doi.org/10.1016/j.devcel.2006.10.002.

14. Misfeldt, A.M., Boyle, S.C., Tompkins, K.L., Bautch, V.L., Labosky, P.A., and Baldwin, H.S. (2009). Endocardial cells are a distinct endothelial lineage derived from Flk1+ multipotent cardiovascular progenitors. Dev. Biol. *333*, 78–89. https://doi.org/10.1016/j.ydbio.2009.06.033.
15. Motoike, T., Markham, D.W., Rossant, J., and Sato, T.N. (2003). Evidence for novel fate of Flk1+ progenitor: Contribution to muscle lineage. Genesis *35*, 153–159. https://doi.org/10.1002/gene.10175.
16. Bu, L., Jiang, X., Martin-Puig, S., Caron, L., Zhu, S., Shao, Y., Roberts, D. J., Huang, P.L., Domian, I.J., and Chien, K.R. (2009). Human ISL1 heart progenitors generate diverse multipotent cardiovascular cell lineages. Nature *460*, 113–117. https://doi.org/10.1038/nature08191.
17. Lee, R.K.K., Stainier, D.Y.R., Weinstein, B.M., and Fishman, M.C. (1994). Cardiovascular development in the zebrafish II. Endocardial progenitors are sequestered within the heart field. Development *120*, 3361–3366. https://doi.org/10.1242/dev.120.12.3361.
18. Milgrom-Hoffman, M., Harrelson, Z., Ferrara, N., Zelzer, E., Evans, S.M., and Tzahor, E. (2011). The heart endocardium is derived from vascular endothelial progenitors. Development *138*, 4777–4787. https://doi.org/10.1242/dev.061192.
19. Bussmann, J., Bakkers, J., and Schulte-Merker, S. (2007). Early endocardial morphogenesis requires Scl/Tal1. PLoS Genet. *3*, e140. https://doi.org/10.1371/journal.pgen.0030140.
20. Schoenebeck, J.J., Keegan, B.R., and Yelon, D. (2007). Vessel and Blood Specification Override Cardiac Potential in Anterior Mesoderm. Dev. Cell *13*, 254–267. https://doi.org/10.1016/j.devcel.2007.05.012.
21. Lioux, G., Liu, X., Temiño, S., Oxendine, M., Ayala, E., Ortega, S., Kelly, R. G., Oliver, G., and Torres, M. (2020). A Second Heart Field-Derived Vasculogenic Niche Contributes to Cardiac Lymphatics. Dev. Cell *52*, 350–363.e6. https://doi.org/10.1016/j.devcel.2019.12.006.
22. Padrón-Barthe, L., Temiño, S., Villa Del Campo, C., Carramolino, L., Isern, J., and Torres, M. (2014). Clonal analysis identifies hemogenic endothelium as the source of the blood-endothelial common lineage in the mouse embryo. Blood *124*, 2523–2532. https://doi.org/10.1182/blood-2013-12-545939.
23. Madisen, L., Zwingman, T.A., Sunkin, S.M., Oh, S.W., Zariwala, H.A., Gu, H., Ng, L.L., Palmiter, R.D., Hawrylycz, M.J., Jones, A.R., et al. (2010). A robust and high-throughput Cre reporting and characterization system for the whole mouse brain. Nat. Neurosci. *13*, 133–140. https://doi.org/10.1038/nn.2467.
24. Sousa, V.H., Miyoshi, G., Hjerling-Leffler, J., Karayannis, T., and Fishell, G. (2009). Characterization of Nkx6-2-derived neocortical interneuron lineages. Cereb. Cortex *19*. i1–10. https://doi.org/10.1093/cercor/bhp038.
25. Guerra, C., Mijimolle, N., Dhawahir, A., Dubus, P., Barradas, M., Serrano, M., Campuzano, V., and Barbacid, M. (2003). Tumor induction by an endogenous K-ras oncogene is highly dependent on cellular context. Cancer Cell *4*, 111–120. https://doi.org/10.1016/S1535-6108(03)00191-0.
26. Vlaeminck-Guillem, V., Carrere, S., Dewitte, F., Stehelin, D., Desbiens, X., and Duterque-Coquillaud, M. (2000). The Ets family member Erg gene is expressed in mesodermal tissues and neural crests at fundamental steps during mouse embryogenesis. Mech. Dev. *91*, 331–335. https://doi.org/10.1016/S0925-4773(99)00272-5.
27. Mittnenzweig, M., Mayshar, Y., Cheng, S., Ben-Yair, R., Hadas, R., Rais, Y., Chomsky, E., Reines, N., Uzonyi, A., Lumerman, L., et al. (2021). A single-embryo, single-cell time-resolved model for mouse gastrulation. Cell *184*, 2825–2842.e22. https://doi.org/10.1016/j.cell.2021.04.004.
28. Solter, D., Škreb, N., and Damjanov, I. (1971). Cell cycle analysis in the mouse egg-cylinder. Exp. Cell Res. *64*, 331–334. https://doi.org/10.1016/0014-4827(71)90084-X.
29. McDole, K., Guignard, L., Amat, F., Berger, A., Malandain, G., Royer, L.A., Turaga, S.C., Branson, K., and Keller, P.J. (2018). In Toto Imaging and Reconstruction of Post-Implantation Mouse Development at the Single-Cell Level. Cell *175*, 859–876.e33. https://doi.org/10.1016/j.cell.2018.09.031.
30. Sendra, M., de Dios Hourcade, J., Temiño, S., Sarabia, A.J., Ocaña, O.H., Domínguez, J.N., and Torres, M. (2023). Cre recombinase microinjection for single-cell tracing and localised gene targeting. Development *150*, dev201206. https://doi.org/10.1242/dev.201206.
31. Ivanovitch, K., Temiño, S., and Torres, M. (2017). Live imaging of heart tube development in mouse reveals alternating phases of cardiac differentiation and morphogenesis. eLife *6*, e30668. https://doi.org/10.7554/eLife.30668.
32. Sendra, M., Mañes, J., Domínguez, J.N., and Torres, M. (2022). Live Imaging of Early Cardiac Progenitors in the Mouse Embryo. J. Vis. Exp. e64273. https://doi.org/10.3791/64273.
33. Muzumdar, M.D., Tasic, B., Miyamichi, K., Li, L., and Luo, L. (2007). A global double-fluorescent cre reporter mouse. Genesis *45*, 593–605. https://doi.org/10.1002/dvg.20335.
34. Nowotschin, S., Xenopoulos, P., Schrode, N., and Hadjantonakis, A.K. (2013). A bright single-cell resolution live imaging reporter of Notch signaling in the mouse. BMC Dev. Biol. *13*, 15. https://doi.org/10.1186/1471-213X-13-15.
35. Wolff, C., Tinevez, J.Y., Pietzsch, T., Stamataki, E., Harich, B., Guignard, L., Preibisch, S., Shorte, S., Keller, P.J., Tomancak, P., et al. (2018). Multi-view light-sheet imaging and tracking with the MaMuT software reveals the cell lineage of a direct developing arthropod limb. eLife *7*, e34410. https://doi.org/10.7554/eLife.34410.
36. Gu, B., Posfai, E., and Rossant, J. (2018). Efficient generation of targeted large insertions by microinjection into two-cell-stage mouse embryos. Nat. Biotechnol. *36*, 632–637. https://doi.org/10.1038/nbt.4166.
37. Tyser, R.C.V., Ibarra-Soria, X., McDole, K., Arcot Jayaram, S., Godwin, J., van den Brand, T.A.H., Miranda, A.M.A., Scialdone, A., Keller, P.J., Marioni, J.C., et al. (2021). Characterization of a common progenitor pool of the epicardium and myocardium. Science *371*, eabb2986. https://doi.org/10.1126/science.abb2986.
38. Zhang, Q., Carlin, D., Zhu, F., Cattaneo, P., Ideker, T., Evans, S.M., Bloomekatz, J., and Chi, N.C. (2021). Unveiling Complexity and Multipotentiality of Early Heart Fields. Circ. Res. *129*, 474–487. https://doi.org/10.1161/CIRCRESAHA.121.318943.
39. Lescroart, F., Wang, X., Lin, X., Swedlund, B., Gargouri, S., Sànchez-Dànes, A., Moignard, V., Dubois, C., Paulissen, C., Kinston, S., et al. (2018). Defining the earliest step of cardiovascular lineage segregation by single-cell RNA-seq. Science *359*, 1177–1181. https://doi.org/10.1126/science.aao4174.
40. Alsan, B.H., and Schultheiss, T.M. (2002). Regulation of avian cardiogenesis by Fgf8 signaling. Development *129*, 1935–1943. https://doi.org/10.1242/dev.129.8.1935.
41. Cai, C.L., Liang, X., Shi, Y., Chu, P.H., Pfaff, S.L., Chen, J., and Evans, S. (2003). Isl1 identifies a cardiac progenitor population that proliferates prior to differentiation and contributes a majority of cells to the heart. Dev. Cell *5*, 877–889. https://doi.org/10.1016/S1534-5807(03)00363-0.
42. Kelly, R.G., Brown, N.A., and Buckingham, M.E. (2001). The Arterial Pole of the Mouse Heart Forms from Fgf10-Expressing Cells in Pharyngeal Mesoderm. Dev. Cell *1*, 435–440. https://doi.org/10.1016/S1534-5807(01)00040-5.
43. Mjaatvedt, C.H., Nakaoka, T., Moreno-Rodriguez, R., Norris, R.A., Kern, M.J., Eisenberg, C.A., Turner, D., and Markwald, R.R. (2001). The outflow tract of the heart is recruited from a novel heart-forming field. Dev. Biol. *238*, 97–109. https://doi.org/10.1006/dbio.2001.0409.
44. Waldo, K.L., Kumiski, D.H., Wallis, K.T., Stadt, H.A., Hutson, M.R., Platt, D. H., and Kirby, M.L. (2001). Conotruncal myocardium arises from a secondary heart field. Development *128*, 3179–3188. https://doi.org/10.1242/dev.128.16.3179.
45. Tam, P.P.L., Parameswaran, M., Kinder, S.J., and Weinberger, R.P. (1997). The allocation of epiblast cells to the embryonic heart and other mesodermal lineages: The role of ingression and tissue movement during gastrulation. Development *124*, 1631–1642. https://doi.org/10.1242/dev.124.9.1631.

46. Garcia-Martinez, V., and Schoenwolf, G.C. (1993). Primitive-streak origin of the cardiovascular system in avian embryos. Dev. Biol. *159*, 706–719. https://doi.org/10.1006/dbio.1993.1276.

47. Peng, G., Suo, S., Chen, J., Chen, W., Liu, C., Yu, F., Wang, R., Chen, S., Sun, N., Cui, G., et al. (2016). Spatial Transcriptome for the Molecular Annotation of Lineage Fates and Cell Identity in Mid-gastrula Mouse Embryo. Dev. Cell *36*, 681–697. https://doi.org/10.1016/j.devcel.2016.02.020.

48. Modat, M., Cash, D.M., Daga, P., Winston, G.P., Duncan, J.S., and Ourselin, S. (2014). Global image registration using a symmetric block-matching approach. J. Med. Imaging (Bellingham) *1*, 024003. https://doi.org/10.1117/1.JMI.1.2.024003.

## STAR★METHODS

### KEY RESOURCES TABLE

| REAGENT or RESOURCE | SOURCE | IDENTIFIER |
|---|---|---|
| Antibodies | | |
| Anti-CD31 (clone MEC 13.3) | BD Pharmingen | Cat# 553370; RRID: AB_394816 |
| Anti-MF20 | Hybridoma Bank | RRID: AB_2147781 |
| Anti-ERG (EPR3863) | Abcam | Cat# Ab110639; RRID: AB_10622193 |
| Anti-N1ICD (Cleaved Notch1 Val1744) | Cell Signaling | Cat# 4147; RRID: AB_2153348 |
| Anti-VEGFR2 | BD Pharmingen | Cat# 555307; RRID: AB_395720 |
| Alexa Fluor 647 goat anti-mouse | Life Technologies | Cat# A31571; RRID: AB_162542 |
| Alexa Fluor 647 goat anti-rat | Life Technologies | Cat# A21247; RRID: AB_141778 |
| Alexa Fluor 594 goat anti-rabbit | Life Technologies | Cat# A11037; RRID: AB_2534095 |
| Biological samples | | |
| Rat Serum culture embryo, male rats SPRAGUE DAWLEY RjHan SD | Janvier Labs | Cat# 9979 |
| Fetal Bovine Serum | Invitrogen | Cat# 10438-026 |
| Chemicals, peptides, and recombinant proteins | | |
| Penicillin-streptomycin | Invitrogen | Cat# 15070-063 |
| 4-Hydroxy Tamoxifen | Sigma | Cat# H7904 |
| TAT-Cre Recombinase | Sigma | Cat# SCR508 |
| DMEM - Dulbecco's Modified Eagle Medium | Gibco | Cat# 10313021 |
| Fluorobrite DMEM | ThermoFisher | Cat# A1896701 |
| Deposited data | | |
| Raw images of 4-Hydroxy Tamoxifen embryo collection | This paper | https://doi.org/10.5281/zenodo.14922060 |
| Raw images of TAT-Cre Recombinase embryo collection | This paper | |
| Raw images Live-imaging datasets | This paper | |
| Clone collection metadata | This paper | Data S1 |
| Experimental models: Organisms/strains | | |
| Mouse: Polr2a–CreERT2 (RERT) *B6;129S-Polr2atm1(cre/ERT2)Bbd/J* | Guerra et al.[25] | JAX strain 017585 |
| Mouse: ROSA26CAG–TdTomato *B6.Cg-Gt(ROSA)26Sortm14(CAG-tdTomato)Hze/J* | Madisen et al.[23] | JAX strain 007914 |
| Mouse: ROSA26CAG–EGFP *B6.129P2-Gt(ROSA)26Sortm2(CAG-EGFP)Fsh/J* | Sousa et al.[24] | N/A |
| Mouse: Tg(CBF:H2BVenus,+) *Tg(Cp-HIST1H2BB/Venus)47Hadj/J* | Nowotschin et al.[34] | JAX strain 020942 |
| Mouse: Tg(H2B:miRFP703,+) | Gu et al.[36] | N/A |
| Mouse: Tg(mT/mG, +) *Gt(ROSA)26Sortm4(ACTB-tdTomato,-EGFP)Luo/J* | Muzumdar et al.[33] | JAX strain 007676 |
| Software and algorithms | | |
| ImageJ | NIH | imagej.nih.gov/ij/ |
| Custom python scripts and notebooks for analysis and plotting | This paper | github.com/MiquelSendra/CardiacLineage |
| LineageTree Library | McDole et al.[29] | github.com/GuignardLab/LineageTree |
| Napari | Napari | napari.org |
| Python version 3.9 | Python Software Foundation | https://www.python.org |
| block–matching registration tools | McDole et al.[29] | github.com/GuignardLab/registration-tools/tree/Alice_Spatial |

(*Continued on next page*)

*Continued*

| REAGENT or RESOURCE | SOURCE | IDENTIFIER |
|---|---|---|
| Other | | |
| Dumont #55 Forceps | Fine Science Tools | Cat# 55 |
| 2% PFA | Merck | Cat# 818715 |
| 35 mm Dish with glass coverslip bottom 14 mm Diameter | Mattek | P35G-1.5-14-C |
| 35 mm vise table | Grandado | SKU 8798771617573 |
| 50 mL tubes | BD Falcon | 352070 |
| Fetal Bovine Serum | Invitrogen | 10438-026 |
| Fluorobrite DMEM | ThermoFisher | A1896701 |
| High-vacuum silicone grease | Dow Corning | Z273554-1EA |
| Holder for wires | Perlen Pressen | pwb1 |
| Penicillin-streptomycin | Invitrogen | 15070-063 |
| Petri dishes 35 × 10 mm | BD Falcon | 351008 |
| Polymethyl methacrylate | This paper | N/A |
| Standard 1.0mm glass capillaries | Anima Lab | 1B100F-3 |
| Sterile 0.22 μm syringe filter | Corning | 431218 |
| Sterile 5 ml syringe | Fisher Scientific | 15809152 |
| LSM 780 Upright microscope | Zeiss | N/A |
| MaiTai Deepsee far red pulsed-laser 980nm | Spectra Physics | N/A |
| Leica TCS SP8 Navigator | Leica | N/A |

## EXPERIMENTAL MODEL AND STUDY PARTICIPANT DETAILS

Mice were handled in accordance with CNIC Ethics Committee, Spanish laws and the EU Directive 2010/63/EU for the use of animals in research. All mouse experiments were approved by the CNIC and Universidad Autónoma de Madrid Committees for "Ética y Bienestar Animal" and the area of "Protección Animal" of the Community of Madrid with reference PROEX 220/15. For this study, mice were maintained on mixed C57Bl/6 or CD1 background. We used the mouse lines stated in the key resources table, which were genotyped by PCR following the original study protocols. Male and female mice of more than 8 weeks of age were used for mating. Mice were housed in specific-pathogen-free facilities at Fundación CNIC and maintained on a 12-h light/12-h darkness schedule, at 45–65% relative humidity and 21–24 °C ambient temperature. Experimental procedures were reviewed and approved by the institutional animal care and use committees at the Centro Nacional de Investigaciones Cardiovasculares (CNIC).

## METHOD DETAILS

### Embryo retrieval

Embryos were staged considering 12:00 on the midday of the vaginal plug as embryonic day (E) 0.5. Females were sacrificed by cervical dislocation. The abdominal cavity of sacrificed females was opened to expose the uterus. The uterus was then placed in ice cold PBS for fixed analysis or in 37°C dissection media for experiments requiring embryo culture (see STAR Methods). After opening the muscle layer and the decidual layer, the embryos were extracted, dissected and finally fixed in paraformaldehyde (PFA, Merck) 2% in PBS overnight at 4°C or placed in pre–equilibrated culture medium.

### Whole mount embryo immunostaining

After fixing embryos in 2% PFA in PBS, immunofluorescence was performed as follows: After three washes with PBS, the embryos were permeabilized with a 0.3% Triton X-100 in PBS solution for 30 minutes at room temperature. Blocking was performed with Bovine Serum Albumine (BSA, Thermo Fisher) 0.5% in PBS for at least 3 hours at 4°C. The primary antibodies were then incubated overnight. We used the following primary antibodies: anti–CD31 (553370 BD Pharmingen clone MECr 13.3), anti– M20 (1:100; Anti–MF–20–mouse Hybridoma bank), anti–ERG (1:500; Anti–ERG antibody Rabbit [EPR3863]–ChiP Grade, Abcam Ab110639), anti-N1ICD (1:1000, Cleaved Notch1 (Val1744) (D3B8) Rabbit mAb #4147, Cell Signaling), anti-VEGFR2 (Purified Rat Anti-Mouse Flk-1 #555307, BD Pharmigen). Primary antibody washing was carried out in a 0.1% Triton X–100 in PBS solution for at least 5 hours at 4°C. Secondary antibody incubation was carried out overnight at 4°C. We used the following secondary antibodies: Alexa Fluor 647 goat anti–mouse (1:500; Life technologies A31571), Alexa Fluor 647 goat anti–rat (1:500; Life technologies A21247) and Alexa Fluor 594 goat anti–rabbit (1:500; Life technologies A11037). All embryos were nuclei stained with DAPI 1:1000 diluted in PBS. Embryos were clarified in crescent dilution of glycerol in PBS (25%, 50% and 75%) until analysis was performed by confocal microscopy.

### Confocal microscopy of fixed embryos

Whole embryos were mounted on 35 mm plates with a 14 mm diameter glass coverslip (Mattek, P35G-1.5-14-C) and imaged on a Leica TCS SP5 confocal microscope using 405, 488, 561, 633 nm wavelengths and 10x/0.4 dry and 20x/0.75 glycerol objectives or on a Leica TCS SP8 confocal microscope using spectral wavelength lasers and nd 20x/0.75 glycerol objectives. A 3D stack was obtained by imaging optical sections every 3 or 5 μm.

For quantification of the Notch reporter expression (CBF1:H2BVenus, +) in the endothelium, we used immunostaining of the CD31 marker. Following confocal imaging, CBF:H2BVenus positive and negative cells were counted within the CD31 positive and negative domains using ImageJ Cell Counter plugin, which output was plotted and statistically analyzed using chi–square test to compare the proportions of positive cells in both domains.

### Retrospective clonal analysis

For retrospective clonal analysis, we used mouse embryos carrying the inducer *Polr2a– CreERT2 (RERT)* and both the reporters *ROSA26CAG–TdTomato* (R26RtdTomato) and *ROSA26CAG–EGFP* (R26REGFP) in trans-heterozygosis. These genotypes were generated upon breeding mice that have the inducer and one of the reporter alleles in double homozygosis with mice that have the second reporter allele in homozygosis. Random Cre–mediated recombination was triggered with 4–hydroxy–tamoxifen dissolved in corn oil. A single dose of 4–hydroxy–tamoxifen was injected intraperitoneally into pregnant females at E5.75 or E6.25 days of gestation. The embryos were dissected, fixed and analyzed at E8.0–E8.5 as described in the following sections.

### Tamoxifen preparation

For induction of the RERT line, 10 mg of 4–hydroxy Tamoxifen (Sigma) was dissolved in 1 ml of absolute ethanol and 9 ml of corn oil (Sigma) for a final concentration of 1 mg/ml. The stock solution was then sonicated for 40 minutes on ice to prevent overheating. The solution was aliquoted and stored at 4°C for up to 4 weeks, and re–sonicated before being administered to mice.

### TAT–Cre prospective clonal analysis

Mouse embryos at developmental stages E6.5 to E7.5 were dissected in a pre-equilibrated medium containing DMEM supplemented with 10% fetal bovine serum, 25 mM HEPES-NaOH (pH 7.2), penicillin, and streptomycin. Subsequently, the embryos were cultured under controlled conditions within a hypoxic chamber incubator at 37°C with 5% O2 and 7% CO2, using a culture medium comprising 50% Janvier Labs Rat Serum SPRAGUE DAWLEY RjHan SD male only and 50% DMEM FluoroBrite. For prospective clonal analysis tracing, embryos in the same developmental range were microinjected with TAT-Cre recombinase using specialized equipment and techniques. Specifically, microinjection needles were prepared with a 2μm gauge and inserted into the anterior side of the embryo until penetrating the endodermal layer, using specified pressure conditions. The embryos were handled and positioned carefully, ensuring that the anterior and posterior sides were oriented accordingly during the procedure to achieve successful microinjections.

In our prospective clonal analysis, we utilized mouse embryos that carried both the reporter genes ROSA26CAG–TdTomato (R26RtdTomato) and ROSA26CAG–EGFP (R26REGFP) in transheterozygosis. Following a process akin to the one used for retrospective clonal analysis, we fixed, imaged, and annotated fluorescent cells within anatomical regions. "Clusters" were defined as groups of cells (either Tomato or GFP) originating from a single TAT-Cre injection. We employed the same probability calculation method as in retrospective clonal analysis, using the two-reporter strategy as previously outlined in the literature.[21,22] Notably, out of 19 clusters analyzed, only one was bicolor, indicating that clusters in the TAT-Cre induced embryo collection had a high likelihood (93%) of being monoclonal.

### Embryo culture and live imaging of gastrulating mouse embryos

Live imaging procedures followed the protocol outlined in Sendra et al.[32] In brief, mouse embryos were carefully collected and dissected within a dissection medium comprised of DMEM supplemented with 10% fetal bovine serum, 25 mM HEPES-NaOH (pH 7.2), and penicillin-streptomycin (50 μg/ml each). For embryos spanning E6.5 to E7.5, culture conditions were established using a mix of 50% Janvier Labs Rat Serum Sprague Dawley RjHan SD (male only) and 50% DMEM FluoroBrite (Thermo Fisher Scientific, A1896701) with incubation at 37°C and a 7% CO2 concentration. Imaging was conducted on a Zeiss LSM780 platform, featuring a 20× objective lens (NA=1) and a MaiTai laser set at 980 nm for two-channel two-photon imaging. Fluorescence was detected with Non Descanned Detectors equipped with the filters cyan-yellow (BP450-500/BP520-560), green-red (BP500-520/BP570-610) and yellow-red (BP520-560/BP645-710). Zen software (Zeiss) facilitated data acquisition with an output power of 250 mW, pixel dwell time of 14.8 s, line averaging of two, and an image dimension of 610×610 μm (1024×1024 pixels).

Embryo MS3 was injected approximately 0.38 nl of undiluted TAT-Cre recombinase ($3.8{\cdot}10^{-r}$ U of TAT-Cre, SCR508, Sigma-Aldrich) using a pneumatic microinjector (Narishige IM 300 Microinjector) 9 psi of injection pressure during 40 ms as previously described.[30] After 3 hours resting in culture media, the embryo was placed in the Zeiss LSM780 platform an imaged as described above.

## QUANTIFICATION AND STATISTICAL ANALYSIS

### Cluster cell counting

Once acquired, the images were opened as optical plane stacks and saved in.tiff format. The contribution of the clusters to each anatomical location was evaluated by counting DAPI nuclei within Tdtomato+ or GFP+ cells. Anatomical locations were identified

using morphological features[1] in the DAPI channel. Additionally, MF20 and ERG immunostaining signal identified cardiomyocytes and endothelial cells. Two overlapping groups of cells (Tomato and GFP cells) were annotated as "bicolor clusters".

The polyclonality of monocolor cell clusters in the embryo collection was estimated using the frequency of bicolor clusters as previously described.[21,22] This method is based in the fact that the frequency of bicolor events in a collection of samples is directly proportional to its polyclonality (Figure III.1A). This allows calculating the probability of finding clusters labeled with one reporter (monocolor clusters) that originate from multiple progenitors (polyclonal) using the following formula (Figure III.1F). We reported previously the relative recombination of GFP and Tdtomato reporter.[30] Briefly, we first estimated the relative Tomato and GFP recombination frequency: *RERT+/-;ROSA26RCAG–TdTomato+/+* mice were crossed with *ROSA26RCAG–GFP+/+* mice. Reporter recombination was induced by administering 0.04 mg/g of 4–OH tamoxifen intraperitoneally to pregnant females on day E7. A day later, the embryos were harvested and the relative efficiency of recombination was calculated by manually counting GFP and TdTomato cells over total DAPI nuclei in confocal optical sections using the ImageJ Cell Counter plugin. We found that Tdtomato recombined 1.97 times as often as GFP.

## Clonal probability

The frequency of mono–color polyclonal clusters can then be estimated as a function of the frequencies of bicolor clusters and of mono–color clusters, which is biased towards the production of Tdtomato clusters, with a calculated frequency of recombination of 1.76% for Tdtomato and 0.87% for GFP (that is, Tdtomato recombines 2.02 times more often). Dismissing polyclonality levels above biclonality and assuming a stochastic distribution of clusters, the following functions apply for estimations:

- Frequency of bicolor clusters = frequency of Tdtomato (A) x frequency of GFP (B) $\times$ 2.
- Frequency of polyclonal monocolor clusters= A2 + B2.
- Then, the frequency of polyclonal monocolor clusters = Frequency of bicolor clusters $\times \frac{1+(A/B)2}{2(A/B)}$

In our case, for the retrospective clonal analysis, 4.5% of the clusters analyzed (2/44) were bicolor. Applying these formulae, we calculated that the clusters in our collection had a 94.3 % chance of being actual clones.

$$1 - \left(\frac{2}{44} \times \frac{1+(1.76/0.87)^2}{2(1.76/0.87)}\right) = 1 - 0.057 = 94.3.$$

## Cell tracking and lineage reconstruction from live imaging data

We used Leo Guignard's lab rigid block–matching registration tools (GitHub repository) developed initially by Grégoire Malandin and Sebastien Ourselin[29,48] and later optimized by Leo Guignard for this project. Block–matching registration corrects translation and rotation in all of the planes. It does so by making blocks of the images and trying to match the intensities between one time point and the next. Subsequently, the blocks are made smaller until optimal matching is found. This corrects for embryo drift and sudden motion between one time point and the next, allowing for the quantification of cell tracking parameters and facilitating tracking itself.

To reconstruct lineages and assess the specification of early cardiac progenitors in our live imaging data, we tracked differentiated cardiomyocytes and endothelial cells located in the cardiac crescent or primitive heart tube back to their initial positions in the nascent mesoderm. Manual cell and lineage annotations were performed using the Fiji plugin Massive Multi-view Tracker (MaMuT).[35] Cells that could not be reliably identified in the previous or following time points were discarded. Once a progenitor was successfully tracked from the beginning to the end of the video, the rest of its sisters were tracked on each division to reconstruct the full lineage. For some cases, sister cell tracks were lost due the cell falling out of frame, moving to an area with poor resolution or crowded with many cells. Next, MaMut output files (parsed.xml in a graph data structure) were processed using a custom python script. This script is available as a Jupyter notebook in our GitHub Repository. Briefly, we used Leo Guignard's LineageTree Python library (GitHub repository) to retrieve cell lineages and XYZ coordinates from the.xml files to plot tracks in 3D and lineage representations.

To represent the location of progenitors on the raw data, we used the open-source software Napari (napari.org) in combination with a custom python script, which is available (GitHub repository). 3D data can be explored for each embryo by installing Napari and loading the raw data and 3D positions all at once using the provided code snippet directly on Napari's terminal, specifying the location of the folder containing the layer's file.

## Probability calculation for clone specification

To assess whether the observed lineage outcomes of clones are due to chance or lineage specification (Figure S6D) we calculated the probabilities of a clone containing cardiomyocytes (CMs) but no endocardial cells (ECrs), and vice versa.

For a clone with $n$ cells in the heart, the probabilities are calculated as follows:

1 Probability of all CM (no ECr)

$$P(\text{all CM}) = (p_{CM})^n$$

Where $p_{CM}$ is the probability of a cell being a CM. This is the ratio of the total number of CM cells to the total number of heart cells (CM + ECr), which in our collection is 0.64.

2 Probability of all ECr (no CM)

$$P(\text{all ECr}) = (p_{ECr})^n$$

where $p_{ECr}$ is the probability of a cell being an ECr. This is the ratio of the total number of ECr cells to the total number of heart cells (CM + ECr), which in our collection is 0.36.

These probabilities were calculated for clones containing more than 4 cells, taking into account its size ($n$) and the known average proportions of CM and ECr in the dataset. This analysis provided an estimate of the likelihood that clones with restricted lineage outcomes occurred by chance.